The Journal of Immunology

Involvement of PARK2-Mediated Mitophagy in Idiopathic Pulmonary Fibrosis Pathogenesis

Kenji Kobayashi, Jun Araya, Shunsuke Minagawa, Hiromichi Hara, Nayuta Saito, Tsukasa Kadota, Nahoko Sato, Masahiro Yoshida, Kazuya Tsubouchi, Yusuke Kurita, Saburo Ito, Yu Fujita, Naoki Takasaka, Hirofumi Utsumi, Haruhiko Yanagisawa, Mitsuo Hashimoto, Hiroshi Wakui, Jun Kojima, Kenichiro Shimizu, Takanori Numata, Makoto Kawaishi, Yumi Kaneko, Hisatoshi Asano, Makoto Yamashita, Makoto Odaka, Toshiaki Morikawa, Katsutoshi Nakayama and Kazuyoshi Kuwano

J Immunol 2016; 197:504-516; Prepublished online 8 June 2016;
doi: 10.4049/jimmunol.1600265
http://www.jimmunol.org/content/197/2/504

The Journal of Immunology is published twice each month by
The American Association of Immunologists, Inc.,
1451 Rockville Pike, Suite 650, Rockville, MD 20852

Print ISSN: 0022-1767 Online ISSN: 1550-6606.

Involvement of PARK2-Mediated Mitophagy in Idiopathic Pulmonary Fibrosis Pathogenesis

Kenji Kobayashi,* Jun Araya,* Shunsuke Minagawa,* Hiromichi Hara,* Nayuta Saito,* Tsukasa Kadota,* Nahoko Sato,* Masahiro Yoshida,* Kazuya Tsubouchi,* Yusuke Kurita,* Saburo Ito,* Yu Fujita,* Naoki Takasaka,* Hirofumi Utsumi,* Haruhiko Yanagisawa,* Mitsuo Hashimoto,* Hiroshi Wakui,* Jun Kojima,* Kenichiro Shimizu,* Takanori Numata,* Makoto Kawaishi,* Yumi Kaneko,* Hisatoshi Asano,† Makoto Yamashita,† Makoto Odaka,† Toshiaki Morikawa,† Katsutoshi Nakayama,* and Kazuyoshi Kuwano*

Fibroblastic foci, known to be the leading edge of fibrosis development in idiopathic pulmonary fibrosis (IPF), are composed of fibrogenic myofibroblasts. Autophagy has been implicated in the regulation of myofibroblast differentiation. Insufficient mitophagy, the mitochondria-selective autophagy, results in increased reactive oxygen species, which may modulate cell signaling pathways for myofibroblast differentiation. Therefore, we sought to investigate the regulatory role of mitophagy in myofibroblast differentiation as a part of IPF pathogenesis. Lung fibroblasts were used in in vitro experiments. Immunohistochemical evaluation in IPF lung tissues was performed. PARK2 was examined as a target molecule for mitophagy regulation, and a PARK2 knockout mouse was employed in a bleomycin-induced lung fibrosis model. We demonstrated that PARK2 knockdown-mediated mitophagy inhibition was involved in the mechanism for activation of the platelet-derived growth factor receptor (PDGFR)/PI3K/AKT signaling pathway accompanied by enhanced myofibroblast differentiation and proliferation, which were clearly inhibited by treatment with both antioxidants and AG1296, a PDGFR inhibitor. Mitophagy inhibition–mediated activation of PDGFR signaling was responsible for further autophagy suppression, suggesting the existence of a self-amplifying loop of mitophagy inhibition and PDGFR activation. IPF lung demonstrated reduced PARK2 with concomitantly increased PDGFR phosphorylation. Furthermore, bleomycin-induced lung fibrosis was enhanced in PARK2 knockout mice and subsequently inhibited by AG1296. These findings suggest that insufficient mitophagy-mediated PDGFR/PI3K/AKT activation, which is mainly attributed to reduced PARK2 expression, is a potent underlying mechanism for myofibroblast differentiation and proliferation in fibroblastic foci formation during IPF pathogenesis. ***The Journal of Immunology*****, 2016, 197: 504–516.**

Idiopathic pulmonary fibrosis (IPF) is a progressive fibrosing interstitial pneumonia of unknown cause (1–3). Fibroblastic foci (FF) comprised of myofibroblasts with excessive extracellular matrix production are recognized to be the leading edge of fibrosis development (4). The cell origin of myofibroblasts remains to be clearly determined, and several different cell types, including tissue-resident mesenchymal cells, bone marrow–derived cells (fibrocytes), epithelial cells, pleural mesothelial cells, and pericytes have been proposed as the precursor, suggesting that heterogeneous cell populations are involved in the formation of the FF (2, 5). Accordingly, not only the cell origin but also the cellular mechanisms for myofibroblast differentiation and proliferation can be critical determinants of FF formation in IPF.

Autophagy is a highly conserved machinery of delivering cytoplasmic components for lysosomal degradation. Proper turnover of damaged organelles is considered to be cytoprotective during the integrated stress response (6, 7). We have reported the potential involvement of insufficient autophagy in IPF pathogenesis through the regulation of both epithelial cell senescence and myofibroblast differentiation (8). Among autophagy-related proteins (ATG) required for autophagosome formation, ATG5 is one of the key regulators of the autophagy process and is critically responsible for autophagosome formation (9). Intriguingly, autophagy inhibition by ATG5 knockdown is sufficient to induce myofibroblast differentiation without supplemental profibrotic growth factors in lung fibroblasts (LF), but the detailed mechanism remains to be elucidated (8).

Reactive oxygen species (ROS) play a pivotal role in myofibroblast differentiation by modulating intracellular signaling pathways (10). Insufficient mitophagy (mitochondria selective autophagy) gives rise to the accumulation of damaged mitochondria with

*Division of Respiratory Diseases, Department of Internal Medicine, Jikei University School of Medicine, Tokyo 105-8461, Japan; and †Division of Chest Diseases, Department of Surgery, Jikei University School of Medicine, Tokyo 105-8461, Japan

ORCIDs: 0000-0002-9533-7241 (T.K.); 0000-0002-8916-7303 (Y.F.).

Received for publication February 16, 2016. Accepted for publication May 13, 2016.

This work was supported by a Jikei University graduate research grant to (to K. Kobayashi, Y. Kurita, S.I., and T. N.), a grant-in-aid for scientific research from the Ministry of Education of Japan (to J.A., H.H., J.K., K.S., K.N., and K. Kuwano), as well as grants from the Satoshi Okamoto Memorial Foundation of Pulmonary Fibrosis (to J.A.), the Practical Research Project for Rare Intractable Diseases from the Japan Agency for Medical Research and Development (to K. Kuwano), and by the Ministry of Health, Labor, and Welfare of Japan awarded to the Study Group on Diffuse Pulmonary Disorders, Scientific Research/Research on Intractable Diseases (to K. Kuwano).

Address correspondence and reprint requests to Dr. Jun Araya, Division of Respiratory Diseases, Department of Internal Medicine, Jikei University School of Medicine, 3-25-8 Nishi-shimbashi, Minato-ku, Tokyo 105-8461, Japan. E-mail address: araya@jikei.ac.jp

The online version of this article contains supplemental material.

Abbreviations used in this article: Baf A1, bafilomycin A1; BLM, bleomycin; DCFH-DA, 2′,7′-dichlorodihydrofluorescein diacetate; FF, fibroblastic focus; IPF, idiopathic pulmonary fibrosis; KO, knockout; LC3, L chain 3; LF, lung fibroblast; MFN, mitofusin; mTOR, mammalian target of rapamycin; NAC, *N*-acetylcysteine; PDGF, platelet-derived growth factor; PDGFR, platelet-derived growth factor receptor; PINK1, PTEN-induced putative protein kinase 1; ROS, reactive oxygen species; siRNA, small interfering RNA; α-SMA, α smooth muscle actin.

www.jimmunol.org/cgi/doi/10.4049/jimmunol.1600265

concomitant production of excessive endogenous ROS. Interestingly, a recent study demonstrated that enhanced mitochondrial ROS resulting from impaired mitophagy was responsible for the persistent activation of platelet-derived growth factor receptor (PDGFR) (11). PDGF has been widely implicated in the pathogenic sequence of IPF development and is involved in the regulation of myofibroblast differentiation and proliferation in various fibrotic disorders (12–15). Thus, we postulate that our recent finding of autophagy inhibition–mediated myofibroblast differentiation can be attributed to increased mitochondrial ROS-mediated activation of PDGF signaling.

The PTEN-induced putative protein kinase 1 (PINK1)/PARK2 pathway participates in mitochondria selective autophagy machinery known as mitophagy, and gene mutations of both *PINK1* and *PARK2* are coupled with Parkinson's disease resulting from accumulation of damaged mitochondria (16). Stress-induced membrane depolarization stabilizes PINK1, leading to recruitment of PARK2 to mitochondria, and PARK2-mediated ubiquitination of mitochondrial substrates is required for mitophagic recognition. Recent studies, including our findings, implicated PINK1- and PARK2-mediated mitophagy in the modulation of lung epithelial cell death and senescence in terms of IPF and chronic obstructive pulmonary disease pathogenesis (17–19). However, the regulatory involvement of mitophagy in phenotypic alterations of fibroblast during lung fibrosis development remains to be elucidated. Hence, we examined the involvement of PARK2-mediated mitophagy in the regulation of the PDGFR signaling pathway and myofibroblast differentiation in LF in the context of IPF pathogenesis.

Materials and Methods

Cell culture, Abs, and reagents

Human lung tissues were obtained from pneumonectomy and lobectomy specimens for primary lung cancer. Informed consent was obtained from all surgical participants as part of an approved ongoing research protocol by the Ethical Committee of Jikei University School of Medicine. LF were isolated and characterized as previously described (20). During the process of normal LF isolation, histological evaluation was performed to exclude the involvement of cancer tissues and ensure that fibroblasts were derived from normal tissues only. LF outgrown from lung fragments were cultured in fibroblast growth media (DMEM with 10% FCS and penicillin-streptomycin). LF were serially passaged and used for experiments until passage 6. LF demonstrated >95% positive staining with anti-vimentin Abs, and <5% positive staining with anti-cytokeratin Ab (data not shown). Abs used were rabbit anti-PARK2 (Cell Signaling Technology, no. 2132 and Abcam, no. 5494), rabbit anti-PINK1 (Cell Signaling Technology, no. 6946 and Abcam, no. 23707), rabbit anti–phospho-PDGFRα (Cell Signaling Technology, no. 2992 and Abcam, no. 5460), rabbit anti-PDGFRα (Santa Cruz Biotechnology, no. 338), mouse anti–phospho-PDGFRβ (Cell Signaling Technology, no. 3166), rabbit anti–phospho-PDGFRβ (Abcam, no. 16868), rabbit anti-PDGFRβ (Cell Signaling Technology, no. 3169), rabbit anti–phospho-PI3K (Cell Signaling Technology, no. 4228), rabbit anti-PI3K (Cell Signaling Technology, no. 4257), rabbit anti–phospho-AKT (Cell Signaling Technology, no. 4060), rabbit anti-AKT (Cell Signaling Technology, no. 4691), rabbit anti–phospho-p70 S6 kinase (Cell Signaling Technology, no. 9205), rabbit anti–p70 S6 kinase (Cell Signaling Technology, no. 9202), rabbit anti–microtubule-associated protein 1A/1B–L chain 3 (LC3) (Novus Biologicals, no. 600-1384), rabbit anti-ATG5 (Cell Signaling Technology, no. 2630), rabbit anti–p62 SQSTM1 (MBL International, no. PM045), rabbit anti-ubiquitin (Enzo Life Sciences, no. BML-PW8810), mouse anti–α smooth muscle actin (α-SMA; Sigma-Aldrich, no. A2547), goat anti–type I collagen (SouthernBiotech, no. 1310-0), rabbit anti–optic atrophy 1 (Novus Biologicals, no. 110-55290), mouse anti-mitofusin (MFN)1 (Abcam, no. 57602), mouse anti-MFN2 (Abcam, no. 56889), rabbit anti–mitochondrial fission 1 protein (Santa Cruz, no. 98900), rabbit anti–dynamin-related protein 1 (Cell Signaling Technology, no. 8570), and mouse anti–β-actin (Sigma-Aldrich, no. A5441). Bafilomycin A1 (Baf A1; Sigma-Aldrich, no. B1793), Torin 1 (Tocris Bioscience, no. 4247), Hoechst 33258 (Sigma-Aldrich, no. B2883), MitoSOX Red (Molecular Probes/Life Technologies, no. M36008), *N*-acetylcysteine (NAC) (Wako, no. 017-05131), Mito-TEMPO (Enzo Life Sciences, no. ALX-430-150), wortmannin (Sigma-Aldrich, no. W1628), Akt1/2 kinase inhibitor (Sigma-Aldrich, no. A6730), AG1296, a PDGFR inhibitor (Calbiochem, no. 658551), BGJ398, a fibroblast growth factor receptor inhibitor (Selleck Chemicals, no. S2183), axitinib, a vascular endothelial growth factor receptor inhibitor (Selleck Chemicals, no. S1005), pepstatin A (Peptide Institute, no. 4397), E64d (Peptide Institute, no. 4321-v), bleomycin (BLM; Nippon Kayaku, Tokyo, Japan), and MitoTracker Red CMXRos (Life Technologies, no. M7512) were purchased.

Plasmids, small interfering RNA, and transfection

The LC3 cDNA was the gift of Dr. N. Mizushima (Tokyo University, Tokyo, Japan) and Dr. T. Yoshimori (Osaka University, Osaka, Japan) and was cloned into the pEGFP-C1 vector (21). Small interfering RNA (siRNA) targeting ATG5 (Applied Biosystems/Life Technologies, nos. s18159 and s18160), PARK2 (Applied Biosystems/Life Technologies, nos. s10043 and s10044), PINK1 (Applied Biosystems/Life Technologies, nos. s35166 and s35167), and negative control siRNAs (Applied Biosystems/Life Technologies, nos. AM4635 and AM4641) were purchased from Life Technologies. Specific knockdowns of ATG5, PARK2, and PINK1 were validated using two different siRNAs. Transfections of LF were performed using the Neon transfection system (Invitrogen/Life Technologies, no. MPK5000), using matched optimized transfection kits (Invitrogen/Life Technologies, no. MPK10096).

Electron Microscopy

Electron microscopy was performed as previously described (19). LF were transfected with siRNA and fixed with 2% glutaraldehyde/0.1 M phosphate buffer (pH 7.4) and in 1% osmium tetroxide/0.1 M phosphate buffer (pH 7.4) after 48 h of incubation and dehydrated with a graded series of ethanol. Fixed LF were then embedded in epoxy resin. Ultrathin sections were stained with uranyl acetate and lead citrate and observed with the Hitachi H-7500 transmission electron microscope (Hitachi, Tokyo, Japan). For quantitative evaluation of mitochondria in LF, 10 image fields (×10,000) were selected for each sample. Mitochondria <1 μm without fusion to other mitochondria were counted as fragmented.

Immunohistochemistry and immunofluorescence staining

Immunohistochemistry evaluation of human and mouse lung tissue and immunofluorescence staining were performed as previously described (8, 20). Lung tissue samples for immunohistochemistry were collected from pneumonectomy and lobectomy specimens performed for primary lung cancer, and tissue cancer involvement was excluded by histological examinations and the existence of a UIP pattern was confirmed. Informed consent was obtained from all surgical participants as part of an approved ongoing research protocol by the Ethical Committee of Jikei University School of Medicine. Immunohistochemical staining was performed as previously described with minor modification on the paraffin-embedded lung tissues (8, 20). Immunofluorescence staining was also performed as previously described (8, 20). LF were transfected with pEGFP-LC3 with a concomitant nonsilencing control siRNA or PARK2 siRNA, and treatment was started at 24 h posttransfection. LF grown on eight-well culture slides were fixed with 4% paraformaldehyde for 15 min followed by permeabilization with 0.03% Triton X-100 (Wako, no. 160-24751) for 60 min. After blocking with 1% BSA (Sigma-Aldrich, no. A2153) for 60 min, the primary and secondary Abs were applied according to the manufacturers' instructions. Confocal laser scanning microscopic analysis (Keyence, BZ-X700) of mitochondria was performed by mouse anti-TOM20 (Santa Cruz Biotechnology, no. 17764) staining (Carl Zeiss Japan, Tokyo, Japan). According to the manufacturer's instructions, MitoTracker Red CMXRos staining was performed.

Measurement of ROS production

LF, at a density of 1×10^4 per well, were seeded in a 96-well microplate. 2′,7′-Dichlorodihydrofluorescein diacetate (DCFH-DA; Cell Biolabs, no. STA-342) or an OxiSelect intracellular ROS assay kit (Cell Biolabs, no. STA-342-5) was used to measure total cellular ROS according to the manufacturers' instructions. After incubation with DCFH-DA (10 μM) for 24 h at 37°C, fluorescence of dichlorofluorescein was measured at an excitation wavelength of 485 nm and an emission wavelength of 535 nm by a fluorescence microplate reader (Infinite F200; Tecan Japan, Kanagawa, Japan). Mitochondrial ROS production was analyzed by MitoSOX Red staining according to the manufacturer's instructions, which was evaluated by fluorescence microscopy (Olympus, Tokyo, Japan and Keyence, BZ-X700).

Western blotting

LF grown on six-well culture plates were lysed in RIPA buffer (Thermo Fisher Scientific, no. 89900) with protease inhibitor mixture (Roche Diagnostics, no. 11697498001) and 1 mM sodium orthovanadate or lysed with Laemmli sample

buffer. Western blotting was performed as previously described (8). For each experiment, equal amounts of total protein were resolved by 7.5–15% SDS-PAGE. After SDS-PAGE, proteins were transferred to polyvinylidene difluoride membrane (Millipore, no. ISEQ00010), and incubation with specific primary Ab was performed for 1 h at 37°C. After washing several times with PBST, the membrane was incubated by anti-rabbit IgG, HRP-linked secondary Ab (Cell Signaling Technology, no. 7074), anti-mouse IgG, HRP-linked secondary Ab (Cell Signaling Technology, no. 7076), or anti-goat IgG, HRP-linked secondary Ab (Bethyl Laboratories, no. A50-100P) followed by chemiluminescence detection (Bio-Rad Laboratories, no. 1705061) with an LAS-4000 UV mini system (Fujifilm, Tokyo, Japan).

MTT assay

The MTT assay was performed according to the manufacturer's instructions (Roche, no. 11465007001).

Mouse models

C57BL/6J (CLEA Japan, Tokyo, Japan) and B6.129S4-Park2^{tm1Shn}/J (The Jackson Laboratory, Bar Harbor, ME) mice were purchased and were maintained in the animal facility at the Jikei University School of Medicine. All experimental procedures were approved by the Jikei University School of Medicine Animal Care Committee. A dose of 2 U/kg BLM (Nippon Kayaku) was intratracheally administered in 50 μl saline. An i.p. dose of AG1296 (0.5 ng/body) or 0.5% DMSO was given on days 8–19. The lungs were removed at day 21 and were used for histological examination and Sircol soluble collagen assay (Biocolor Life Science Assays, no. S1000). For histological examination, the lungs were fixed overnight in 10% buffered formalin, embedded in paraffin, and sections stained with H&E and Masson trichrome according to conventional methods for histopathological evaluation. Immunohistochemistry was performed as previously described (8, 20). Quantitative measure of Masson trichrome staining was performed by using ImageJ, an open source image processing program. For quantitatively monitoring collagen production in mouse lung, a Sircol soluble collagen assay of left lungs was performed according to the manufacturer's instructions.

TUNEL staining

TUNEL was performed using a DeadEnd fluorometric TUNEL system (Promega, no. G3250) according to the manufacturer's instructions. The TUNEL$^+$ cells in lung were detected using fluorescence microscopy (Nikon, Tokyo, Japan). The number of apoptotic cells was assessed by manual counting of all TUNEL$^+$ cells in each lung (100×).

Measurement of cellular ATP level

ATP levels in cell lysates were measured using a CellTiter-Glo luminescent cell viability assay (Promega, no. G755A and G756A).

Statistical analysis

Data are shown as the average (±SEM) taken from at least three independent experiments. A Student *t* test was used for comparison of two data sets; ANOVA was used for multiple data sets. A Tukey or Dunn test was used for parametric and nonparametric data, respectively, to find where the differences lie. Significance was defined as $p < 0.05$. Statistical software used was Prism version 5 (GraphPad Software, San Diego, CA).

Results

ATG5 knockdown induces mitochondrial ROS production, activation of the PDGFRs/PI3K/AKT signaling pathway, and myofibroblast differentiation in LF

In line with our recent findings (8), ATG5 knockdown-mediated autophagy inhibition is sufficient to induce myofibroblast differentiation of type I collagen and α-SMA expression, which were comparable levels to TGF-β treatment (Fig. 1A). To elucidate the mechanisms for autophagic regulation of myofibroblast differentiation, we focused on mitochondrial ROS. Increased ROS production as measured by DCFH-DA assay for total ROS (increased to 1.51-fold on average) ($p = 0.0274$, Fig. 1B) and MitoSOX Red staining for mitochondrial ROS (Fig. 1C) was shown during ATG5 knockdown.

ROS can act as both an upstream and downstream mediator of PDGFR phosphorylation, and the involvement of mitochondrial ROS in PDGFR activation has been reported in cases of autophagy inhibition (22). Furthermore, PI3K/AKT activation (which is downstream of the PDGFR signaling pathway) participates in the regulation of myofibroblast differentiation (23, 24). ATG5 knockdown-mediated activation of the PDGFRs/PI3K/AKT signaling pathway was elucidated by the detection of phosphorylated forms of PDGFRs, PI3K, and AKT by Western blotting (Fig. 1D, 1E). Phosphorylation was observed at both 48 and 72 h after siRNA transfection (data not shown), suggesting the persistent nature of activation of the PDGFRs signaling pathway. Both NAC (an efficient antioxidant for intracellular ROS) and Mito-TEMPO (a specific antioxidant for mitochondrial ROS) efficiently inhibited the phosphorylation of the PDGFRs/PI3K/AKT signaling pathway and also α-SMA expression ($p < 0.05$, Fig. 1D), indicating the involvement of mitochondrial ROS. The participation of the PI3K/AKT signaling pathway in α-SMA expression during autophagy inhibition was confirmed using wortmannin (PI3K inhibitor) and AKT1/2 inhibitor, respectively ($p < 0.05$, Fig. 1E). Intriguingly, wortmannin reduced phosphorylation of PDGFRs and AKT1/2 inhibitor attenuated phosphorylation of PDGFRs/PI3K, suggesting the existence of a self-amplifying loop in the PDGFRs/PI3K/AKT signaling pathway enabling persistent PDGFRs activation.

Compared with PINK1, PARK2 dominantly regulates myofibroblast differentiation in LF

We next focused on mitochondria selective autophagy (mitophagy), and the PINK1-PARK2 system has been widely implicated in degradation of damaged mitochondria (25). To elucidate the involvement of PINK1 and PARK2 in the regulation of myofibroblast differentiation with respect to type I collagen and α-SMA expression, we employed siRNAs, and efficient knockdown was observed by Western blotting (mean values of relative expression to control siRNA: PINK1 siRNA 0.57 versus PARK2 siRNA 0.53; $p < 0.05$; Fig. 2A, 2B). Although almost equally efficient knockdown by siRNA was observed in both PINK1 and PARK2, PARK2 knockdown induced myofibroblast differentiation more efficiently than that observed by PINK1 knockdown (mean values of relative expression to control siRNA: type I collagen, PINK1 siRNA 1.14 versus PARK2 siRNA 1.36; α-SMA, PINK1 siRNA 2.20 versus PARK2 siRNA 4.33; $p < 0.05$; Fig. 2C). In comparison with PARK2 knockdown, concomitant PINK1 and PARK2 knockdown showed no significant additive effect on myofibroblast differentiation (mean values of relative expression to control siRNA: type I collagen, PINK1 siRNA plus PARK2 siRNA 1.43; α-SMA, PINK1 siRNA plus PARK2 siRNA 4.75; Fig. 2C). Hence, PARK2 was chosen to further study the mechanisms of myofibroblast differentiation during impaired mitophagy in LF.

To confirm the involvement of PARK2 in mitophagy in LF, we used LF expressing EGFP-LC3 (microtubule-associated protein 1A/1B–LC3). Mitophagy was assessed by using confocal microscopy to measure colocalization between TOM20-stained mitochondria and EGFP-LC3 dots as a representation of autophagosome formation. Baf A1, an inhibitor of autolysosomal maturation, alone induced EGFP-LC3 dot formation accompanied by colocalization with TOM20-stained mitochondria (yellow dots), indicating baseline mitophagy in LF (Fig. 2D). PARK2 siRNA–transfected LF demonstrated a marked decrease in colocalization of TOM20-stained mitochondria and EGFP-LC3 dots, indicating the essential role of PARK2 in mitophagy machinery in LF (Fig. 2D).

PARK2 regulates mitochondrial ROS production, activation of the PDGFRs/PI3K/AKT signaling pathway, and α-SMA expression in LF

Consistent with the results of ATG5 knockdown experiments, PARK2 knockdown also increased ROS production (increased to 1.33-fold on average) ($p = 0.0049$, Fig. 3A), reflecting insufficient mitophagic degradation of damaged mitochondria with enhanced

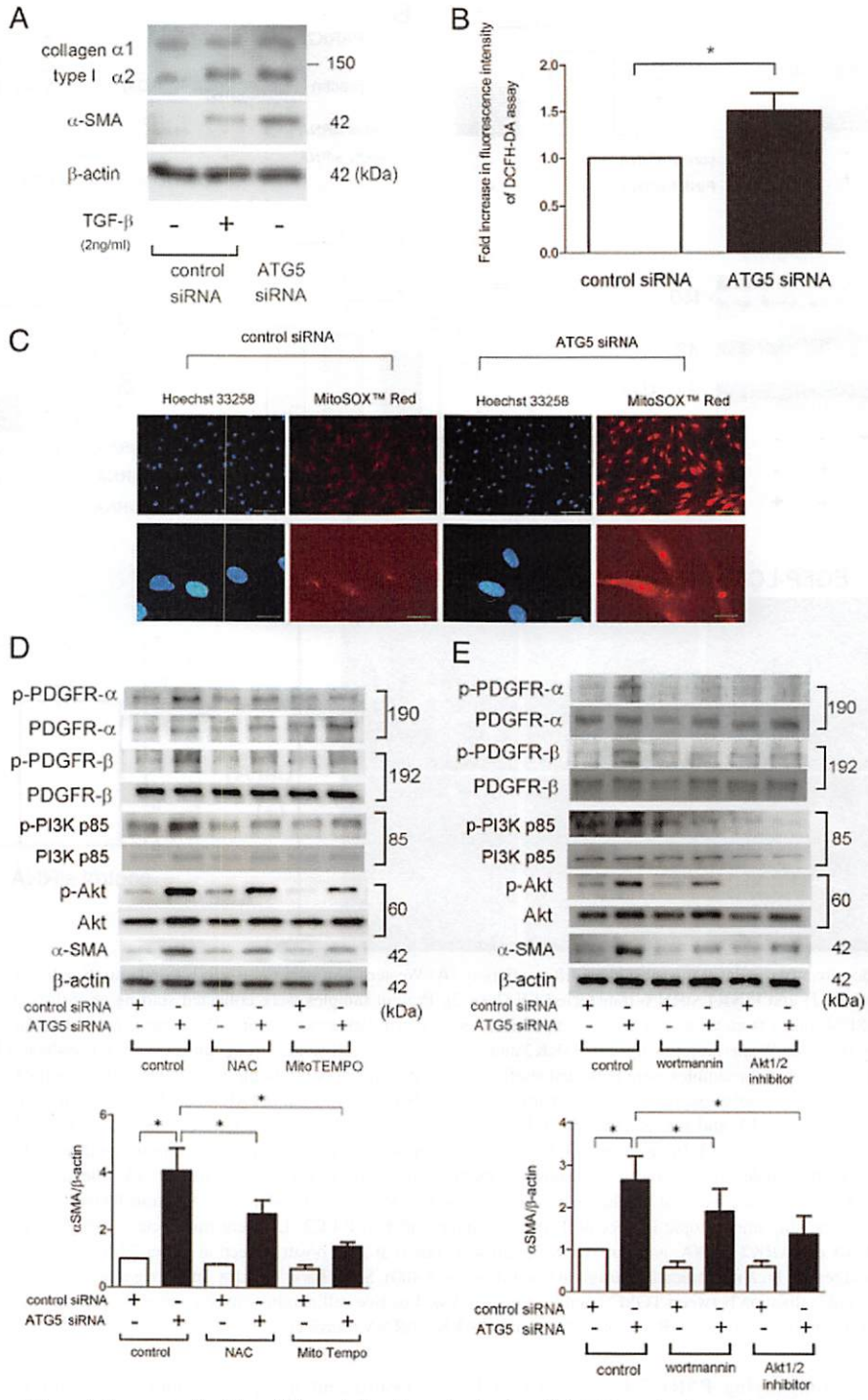

FIGURE 1. ATG5 knockdown induces myofibroblast differentiation through mitochondrial ROS production and activation of the PDGFRs/PI3K/AKT signaling pathway. (**A**) Western blot using anti–type 1 collagen, anti–α-SMA, and anti–β-actin of cell lysates from control siRNA–transfected LF (*lanes 1* and *2*) and ATG5 siRNA–transfected LF (*lane 3*). TGF-β treatment (2 ng/ml) was started at 24 h posttransfection (*lane 2*) and protein samples were collected after 24 h of treatment. (**B**) Fluorescence intensity of DCFH-DA staining for intracellular ROS production. Incubation with DCFH-DA was started at 48 h after siRNA transfection in LF. The fluorescence level in the control siRNA–transfected cells was designated as a 1.0. $*p < 0.05$. (**C**) Images of Hoechst 33258 and MitoSOX Red fluorescence staining in LF. LF were transfected with nonsilencing control siRNA and ATG5 siRNA, and staining was performed 48 h after siRNA transfection. Scale bars, 100 μm (*upper panels*) and 20 μm (*lower panels*). (**D**) Western blot using anti–phospho-PDGFR-α (p-PDGFR-α), anti–PDGFR-α, anti–phospho-PDGFR-β (p-PDGFR-β), anti–PDGFR-β, anti–phospho-PI3K p85 (p-PI3K p85), anti– PI3K p85, anti–phospho-AKT (p-AKT), anti-AKT, anti–α-SMA, and anti–β-actin of cell lysates from control siRNA–transfected LF (*lanes 1*, *3*, and *5*) and ATG5 siRNA–transfected LF (*lanes 2*, *4*, and *6*). NAC (1 mM) and Mito-TEMPO (100 μM) treatments were started at 24 h posttransfection and protein samples were collected after 24 h of treatment. In the *lower panel* is the average (±SEM) taken from three independent experiments shown as relative expressions of α-SMA. Open bar is control siRNA and filled bar is ATG5 siRNA transfected. $*p < 0.05$. (**E**) Western blot using anti–p-PDGFR-α, anti-PDGFR-α, anti–p-PDGFR-β, anti–PDGFR-β, anti–p-PI3K p85, anti–PI3K p85, anti–p-AKT, anti-AKT, anti–α-SMA, and anti–β-actin of cell lysates from control siRNA–transfected LF (*lanes 1*, *3*, and *5*) and ATG5 siRNA–transfected LF (*lanes 2*, *4*, and *6*). Wortmannin (10 μM) and AKT1/2 (*Figure legend continues*)

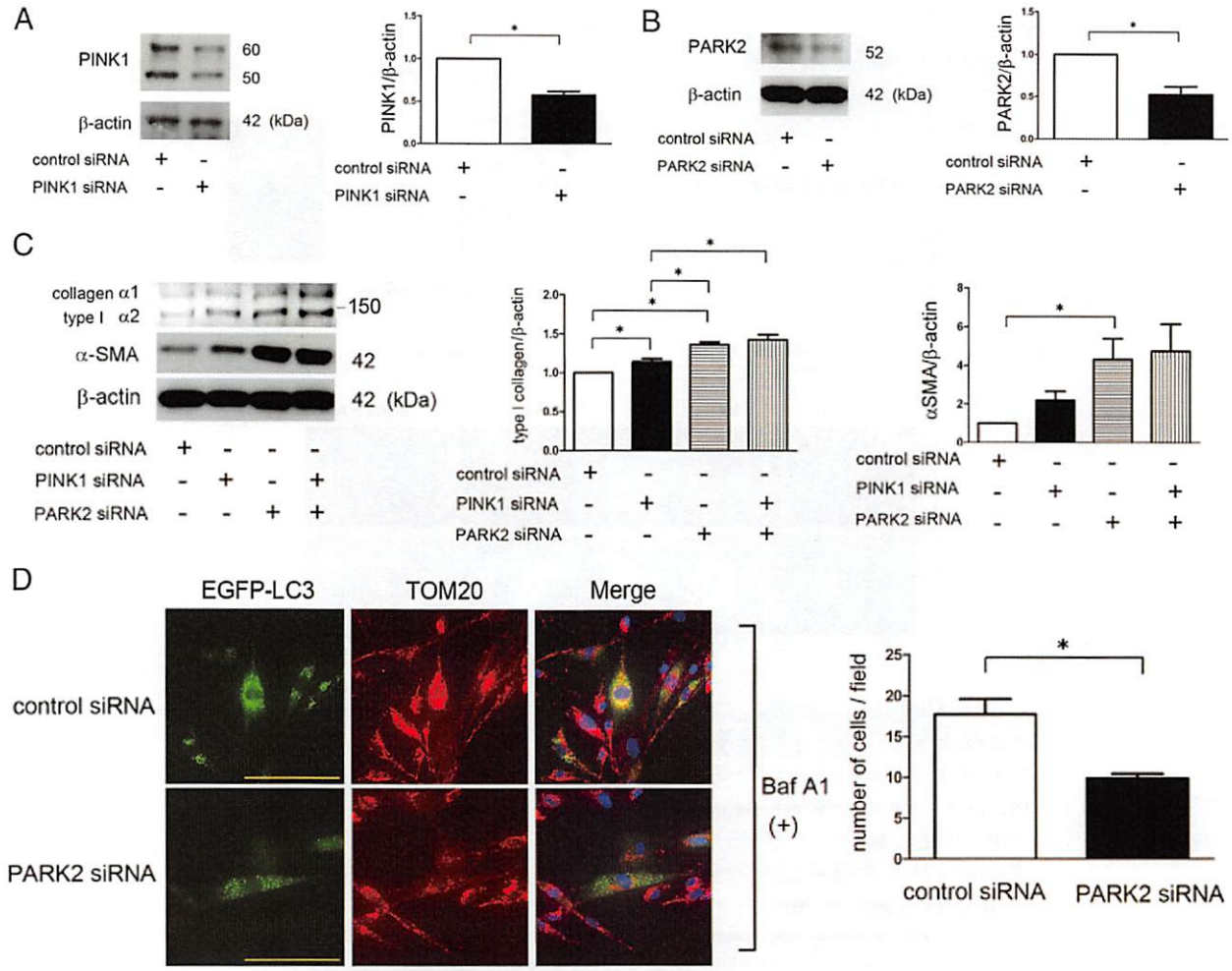

FIGURE 2. PARK2 dominantly regulates myofibroblast differentiation. (**A**) Western blot using anti-PINK1 and anti–β-actin of cell lysates from control siRNA–transfected LF (*lane 1*) and PINK1 siRNA–transfected LF (*lane 2*). Protein samples were collected starting at 48 h posttransfection. In the *right panel* is the average (±SEM) taken from three independent experiments shown as relative expressions. Open bar is control siRNA and filled bar is PINK1 siRNA transfected. $*p < 0.05$. (**B**) Western blot using anti-PARK2 and anti–β-actin of cell lysates from control siRNA–transfected LF (*lane 1*) and PARK2 siRNA–transfected LF (*lane 2*). Protein samples were collected starting at 48 h posttransfection. In the *right panel* is the average (±SEM) taken from three independent experiments shown as relative expressions. Open bar is control siRNA and filled bar is PARK2 siRNA transfected. $*p < 0.05$. (**C**) Western blot using anti–type I collagen, anti–α-SMA, and anti–β-actin of cell lysates from control siRNA–transfected LF (*lane 1*), PINK1 siRNA–transfected LF (*lanes 2* and *4*), and PARK2 siRNA–transfected LF (*lanes 3* and *4*). Protein samples were collected starting at 48 h posttransfection. In the *lower panels* are the average (±SEM) taken from three independent experiments shown as relative expression. Open bar is control siRNA, filled bar is PINK1 siRNA, horizontal crosshatched bar is PARK2 siRNA, and vertical hatched bar is combination of PINK1 and PARK2 siRNA–transfected. $*p < 0.05$. (**D**) Colocalization analysis of confocal laser scanning microscopic images of TOM20 staining and EGFP-LC3. LF were transfected with pEGFP-LC3 with a concomitant nonsilencing control siRNA or PARK2 siRNA, and Baf A1 treatment was started at 24 h posttransfection. After 24 h of treatment with Baf A1, LF were fixed for staining. The images are high magnification (original magnification ×400). Scale bars, 100 μm. In the *right panel* is the average number (±SEM) of cells showing positive colocalization between TOM20 and EGFP-LC3 dots. Positive cell numbers were counted in each image (100×) taken from seven randomly selected areas. Open bar is control siRNA and filled bar is PARK2 siRNA transfected. $*p < 0.05$.

mitochondrial ROS accompanying PARK2 knockdown in LF (Fig. 3B). Furthermore, PARK2 knockdown also induced activation of the the PDGFRs/PI3K/AKT signaling pathway as well as α-SMA expression, which were inhibited by both NAC and Mito-TEMPO ($p < 0.05$, Fig. 3C). PARK2 knockdown-mediated α-SMA expression was also efficiently inhibited by both wortmannin and AKT1/2 inhibitor ($p < 0.05$, Fig. 3D). Wortmannin reduced phosphorylation of PDGFRs, and AKT1/2 inhibitor attenuated phosphorylation of PDGFR/PI3K (Fig. 3D), supporting the notion that insufficient mitophagy induces self-amplifying activation of the the PDGFRs/PI3K/AKT signaling pathway.

PDGFRs activation is involved in α-SMA in LF resulting from insufficient autophagy/mitophagy

To clarify whether autophagy/mitophagy inhibition-mediated PDGFR activation is specifically responsible for myofibroblast differentiation, we employed AG1296, a PDGFR inhibitor, BGJ398, a fibroblast growth factor receptor inhibitor, and axitinib, a vascular endothelial

inhibitor (5 μM) treatments were started at 24 h posttransfection and protein samples were collected after 24 h of treatment. In the *lower panel* is the average (±SEM) taken from three independent experiments shown as relative expressions of α-SMA. Open bar is control siRNA and filled bar is ATG5 siRNA transfected. $*p < 0.05$.

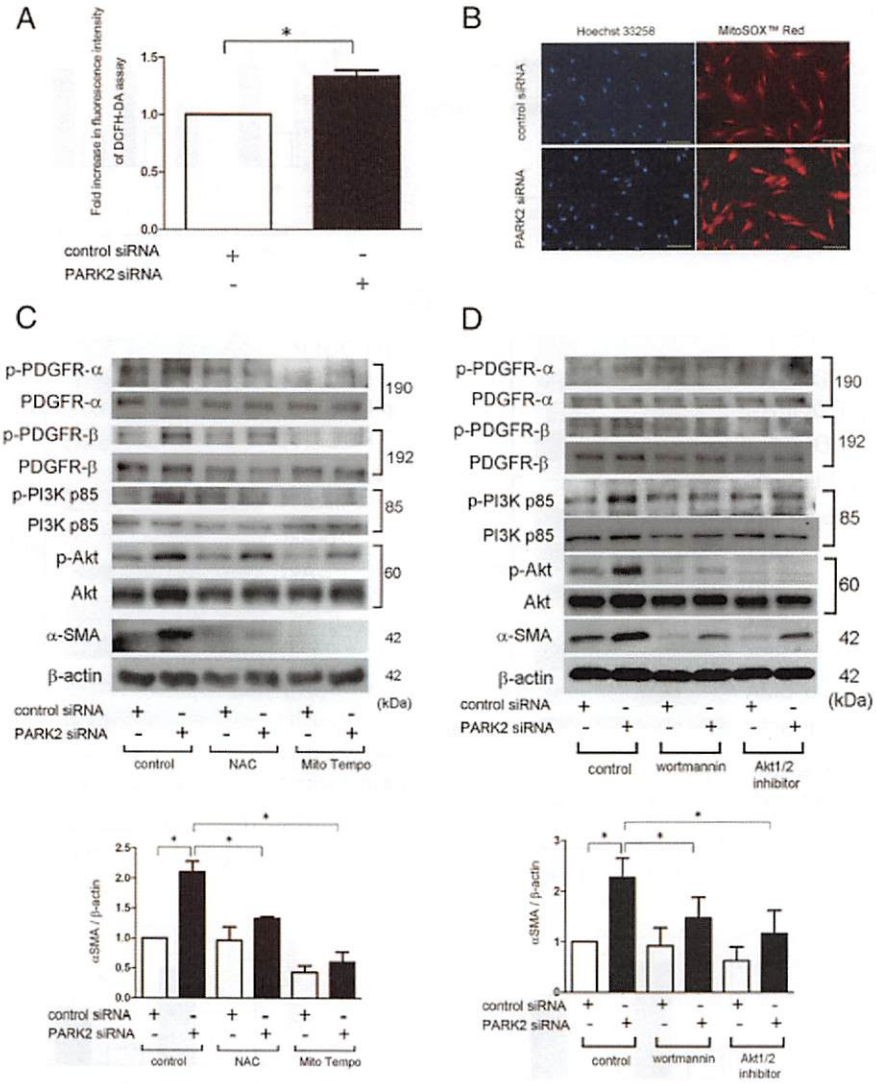

FIGURE 3. PARK2 knockdown induces α-SMA expression through mitochondrial ROS production and activation of the PDGFRs/PI3K/AKT signaling pathway. (**A**) Fluorescence intensity of DCFH-DA staining for intracellular ROS production. Incubation with DCFH-DA was started at 48 h after siRNA transfection in LF. The fluorescence level in the control siRNA–transfected cells was designated as a 1.0. $*p < 0.05$. (**B**) Images of Hoechst 33258 and MitoSOX Red fluorescence staining in LF. LF were transfected with nonsilencing control siRNA and PARK2 siRNA, and staining was performed 48 h after siRNA transfection. Scale bars, 100 μm. (**C**) Western blot using anti–p-PDGFR-α, anti–PDGFR-α, anti–p-PDGFR-β, anti–PDGFR-β, anti–p-PI3K p85, anti–PI3K p85, anti–p-AKT, anti-AKT, anti–α-SMA, and anti–β-actin of cell lysates from control siRNA–transfected LF (*lanes 1*, *3*, and *5*) and PARK2 siRNA–transfected LF (*lanes 2*, *4*, and *6*). NAC (1 mM) and Mito-TEMPO (100 μM) treatments were started at 24 h posttransfection and protein samples were collected after 24 h of treatment. In the *lower panel* is the average (±SEM) taken from three independent experiments shown as relative expressions of α-SMA. Open bar is control siRNA and filled bar is PARK2 siRNA transfected. $*p < 0.05$. (**D**) Western blot using anti–p-PDGFR-α, anti–PDGFR-α, anti–p-PDGFR-β, anti–PDGFR-β, anti–p-PI3K p85, anti–PI3K p85, anti–p-AKT, anti-AKT, anti–α-SMA, and anti–β-actin of cell lysates from control siRNA–transfected LF (*lanes 1*, *3*, and *5*) and PARK2 siRNA–transfected LF (*lanes 2*, *4*, and *6*). Wortmannin (10 μM) and AKT1/2 inhibitor (5 μM) treatments were started at 24 h posttransfection and protein samples were collected after 24 h of treatment. In the *lower panel* is the average (±SEM) taken from three independent experiments shown as relative expressions of α-SMA. Open bar is control siRNA and filled bar is PARK2 siRNA transfected. $*p < 0.05$.

growth factor receptor inhibitor, respectively. AG1296 but not BGJ398 and axitinib demonstrated significant inhibition of ATG5 knockdown-induced α-SMA expression ($p = 0.019$, Fig. 4A, right panel) and phosphorylation of the PDGFRs/PI3K/AKT signaling pathway (Fig. 4B) ($p < 0.05$, Fig. 4B, *lower panel*). AG1296 was also employed in PARK2 knockdown experiments. AG1296 efficiently inhibited phosphorylation of the PDGFRs/PI3K/AKT signaling pathway (Fig. 4C) and also α-SMA expression induced by PARK2 knockdown ($p < 0.05$, Fig. 4C, *lower panel*), indicating that activation of the PDGFRs signaling pathway is mainly responsible for myofibroblast differentiation of α-SMA expression in LF mediated by insufficient mitophagy/autophagy.

Mammalian target of rapamycin (mTOR) activation, a downstream target of the PDGFR signaling pathway, is a representative negative regulator for autophagy, and hence we speculate that mitophagy inhibition-mediated PDGFRs/mTOR activation further inhibits autophagy/mitophagy, which might constitute part of a self-amplifying loop for PDGFRs activation. Phosphorylated forms of p70 S6 kinase (a downstream signaling molecule of mTOR) was detected by knockdown of ATG5 and PARK2 (Fig. 4B, 4C). Autophagy activation was evaluated by detecting the conversion of LC3 from LC3-I (free form) to LC3-II (phosphatidylethanolamine-conjugated form) in the presence of protease inhibitors (E64d and pepstatin A). PARK2 knockdown significantly reduced

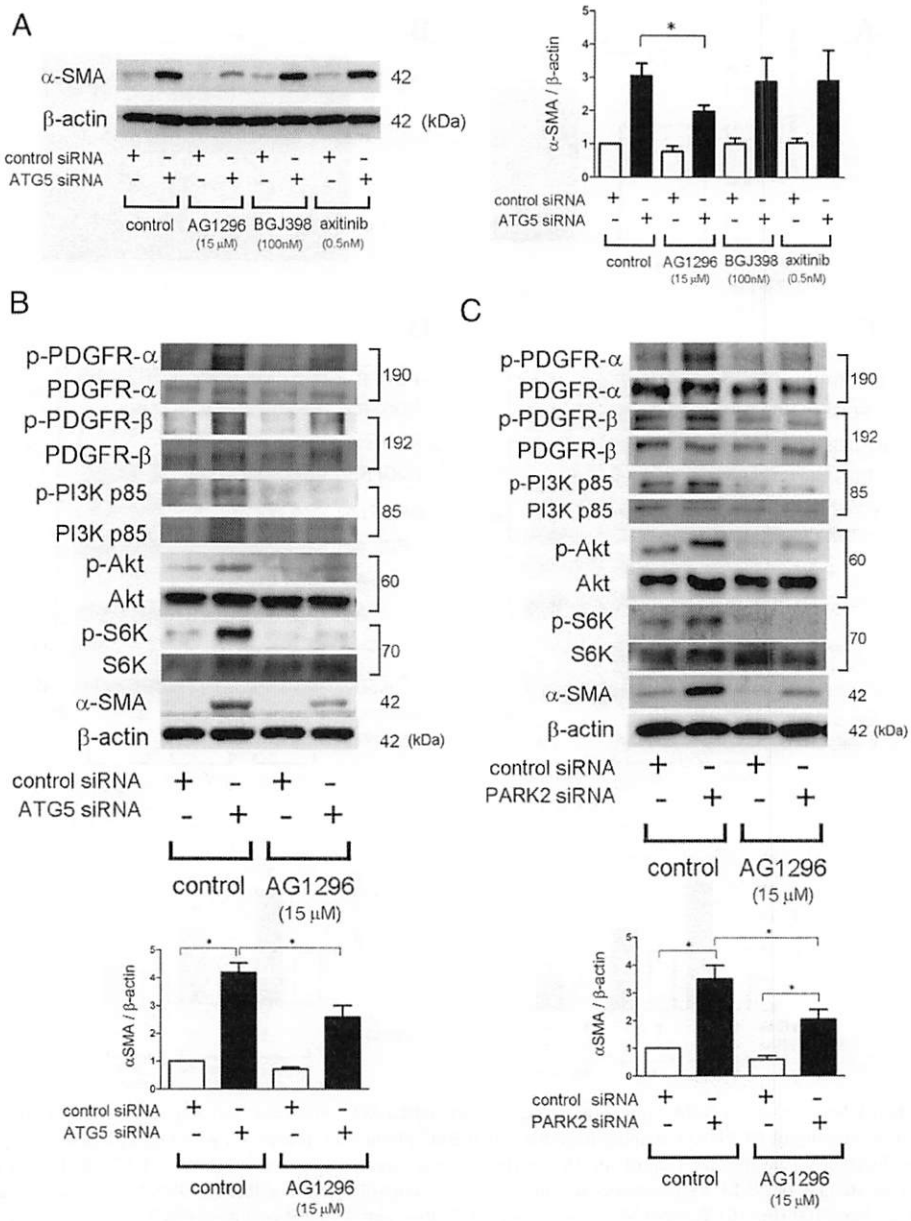

FIGURE 4. AG1296 suppresses ATG5 and PARK2 knockdown-induced α-SMA expression and activation of the PDGFR/PI3K/AKT signaling pathway. (**A**) Western blot using anti–α-SMA and anti–β-actin of cell lysates from control siRNA–transfected LF (*lanes 1*, *3*, *5*, and 7) and ATG5 siRNA–transfected LF (*lanes 2*, *4*, *6*, and *8*). AG1296 (15 μM), BGJ398 (100 nM), and axitinib (0.5 nM) treatments were started at 24 h posttransfection and protein samples were collected after 24 h of treatment. *Right panel* is the average (±SEM) taken from three independent experiments shown as relative expression. Open bar is control siRNA and filled bar is ATG5 siRNA transfected. $*p < 0.05$. (**B**) Western blot using anti–p-PDGFR-α, anti–PDGFR-α, anti–p-PDGFR-β, anti–PDGFR-β, anti–p-PI3K p85, anti–PI3K p85, anti–p-AKT, anti-AKT, anti–p-p70 S6 kinase (p-S6K), anti-S6K, anti–α-SMA, and anti–β-actin of cell lysates from control siRNA–transfected LF (*lanes 1* and *3*) and ATG5 siRNA–transfected LF (*lanes 2* and *4*). AG1296 (15 μM) treatment was started at 24 h posttransfection and protein samples were collected after 24 h of treatment. In the *lower panel* is the average (±SEM) taken from three independent experiments shown as relative expressions of α-SMA. Open bar is control siRNA and filled bar is ATG5 siRNA transfected. $*p < 0.05$. (**C**) Western blot using anti–p-PDGFR-α, anti–PDGFR-α, anti–p-PDGFR-β, anti–PDGFR-β, anti–p-PI3K p85, anti–PI3K p85, anti–p-AKT, anti-AKT, anti–p-S6K, anti-S6K, anti–α-SMA, and anti–β-actin of cell lysates from control siRNA–transfected LF (*lanes 1* and *3*) and PARK2 siRNA–transfected LF (*lanes 2* and *4*). AG1296 (15 μM) treatment was started at 24 h posttransfection and protein samples were collected after 24 h of treatment. In the *lower panel* is the average (±SEM) taken from three independent experiments shown as relative expressions of α-SMA. Open bar is control siRNA and filled bar is PARK2 siRNA transfected. S6K, p70 S6 kinase. $*p < 0.05$.

autophagy activation of LC3 conversion, which was clearly reversed by treatment with AG1296 ($p < 0.05$, Fig. 5A, *right panel*). PARK2 knockdown-mediated autophagy regulation was further confirmed by detecting concomitant changes of p62 and ubiquitinated protein accumulations, which appeared to reflect autophagic degradation ($p < 0.05$, Fig. 5B, *right panels*).

Alteration of mitochondrial structure and myofibroblast proliferation by ATG5 and PARK2 knockdown in LF

Mitochondria are highly dynamic organelles undergoing continuous fusion and fission cycles (26, 27). Fusion rescues mitochondria by redistributing damaged components, and fragmentation of damaged mitochondria results in mitophagic elimination (28). Hence, to clarify

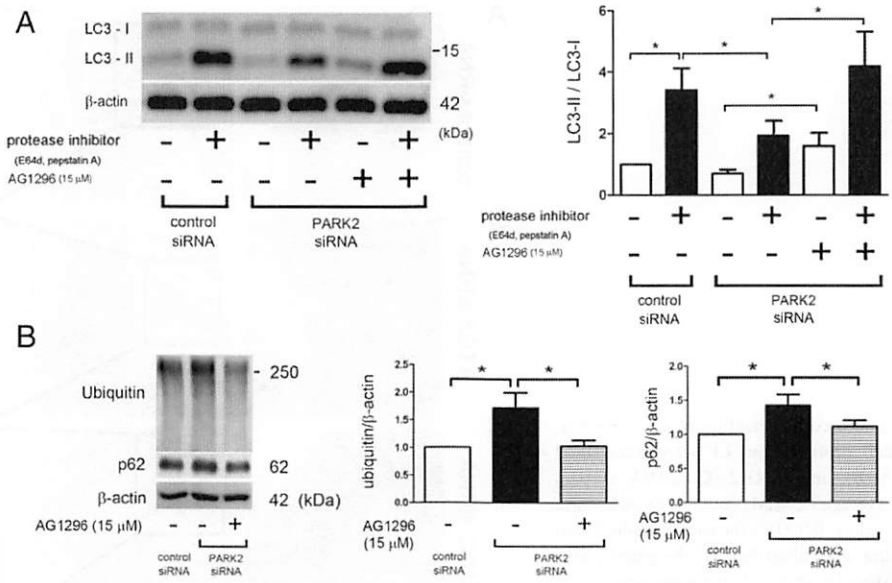

FIGURE 5. AG1296 inhibits PARK2 knockdown-induced autophagy reduction. (**A**) Western blot using anti-LC3 and anti–β-actin of cell lysates from control siRNA–transfected LF (*lanes 1* and *2*) and PARK2 siRNA–transfected LF (*lanes 3–6*) in the presence or absence of protease inhibitors (E64d, pepstatin A). AG1296 (15 μM) treatment was started at 24 h posttransfection and protein samples were collected after 48 h of treatment. In the *right panel* is the average (±SEM) taken from three independent experiments shown as relative expression. Open bar is control and filled bar is protease inhibitor treated. $*p < 0.05$. (**B**) Western blot using anti-ubiquitin, anti-p62, and anti–β-actin of cell lysates from control siRNA–transfected LF (*lane 1*) and PARK2 siRNA–transfected LF (*lanes 2* and *3*). AG1296 (15 μM) treatment was started at 24 h posttransfection and protein samples were collected after 48 h of treatment. In the *right panels* are the averages (±SEM) taken from six independent experiments shown as relative expression. Open bar is control siRNA, filled bar is PARK2 siRNA, and horizontal crosshatched bar is PARK2 siRNA transfected with AG1296 treatment. $*p < 0.05$.

the potential alteration of mitochondrial structure in the setting of insufficient mitophagy in LF, we performed electron microscopy evaluation. Compared to control siRNA–transfected LF, ATG5 and PARK2 knockdown tended to increase both total and elongated mitochondria counts, but significant increase was observed only in counts of elongated mitochondria (Fig. 6A–D) (mean count of elongated mitochondria per field: control siRNA 2.33 versus ATG5 siRNA 3.83 versus PARK2 siRNA 4.92, $p < 0.05$, Fig. 6D). No apparent increase in mitochondrial damage, represented by crista disruption and swelling, was observed in the setting of ATG5 and PARK2 knockdown. To elucidate the mechanism of mitochondrial elongation, we examined fusion-promoting proteins, including optic atrophy 1 and MFN, and also fission-promoting proteins, including dynamin-related protein 1 and mitochondrial fission 1 protein. However, no significant changes in expression levels in total cell lysates were demonstrated by PARK2 knockdown (Supplemental Fig. 1). Not only were mitochondria morphologically intact, but mitochondrial ATP production was not hampered by ATG5 and PARK2 knockdown (Fig. 6E). To further confirm the maintenance in integrity of mitochondrial membrane potential during insufficient mitophagy, MitoTracker Red staining was performed. We detected no apparent difference in intensity of MitoTracker Red staining between control siRNA– and PARK2 siRNA–transfected LF (Fig. 6F). Accordingly, it is likely that mitochondrial elongation via an enhanced fusion process rescued mitochondria from insufficient mitophagy and maintained functional energy production during myofibroblast differentiation in LF.

Both myofibroblast differentiation and proliferation are crucial processes for fibrosis development in IPF. An MTT assay was performed to examine the LF proliferation during insufficient mitophagy. ATG5 and PARK2 knockdown significantly increased the number of LF (ATG5 siRNA, increased to 1.28-fold on average, $p = 0.002$, Fig. 6G; and PARK2 siRNA, increased to 1.20-fold on average, $p = 0.0029$, Fig. 6H), which was efficiently inhibited by NAC and more efficiently by Mito-TEMPO treatment, suggesting that impaired mitophagy-mediated mitochondrial ROS is responsible for cell proliferation ($p < 0.05$, Fig. 6G, 6H). Inhibition of PDGFRs signaling by treatment with AG1296 also inhibited myofibroblast proliferation ($p < 0.05$, Fig. 6G, 6H).

PARK2 and PDGFRs expression in IPF lung

To demonstrate the physiological involvement of PARK2-mediated mitophagy and PDGFRs activation in IPF pathogenesis, expression levels of PARK2, PINK1, p62, ubiquitinated protein, and phosphorylated forms of PDGFRs were assessed by means of immunohistochemical evaluations of FF in IPF lung. In comparison with metaplastic epithelial cells covering FF, fibroblasts constituting FF exhibited barely detectable PARK2 expression (Fig. 7A). In line with our recent findings, FF demonstrated concomitant accumulations of p62 and ubiquitinated proteins (Fig. 7A) (8). Furthermore, in contrast to barely detectable PARK2 expression, increased expression of phosphorylated forms of PDGFRs was present in FF (Fig. 7A).

We next examined the expression levels of PARK2/PINK1, ubiquitinated proteins, p62, and and PDGFRs by Western blot using isolated LF from patient lungs (Table I). Consistent with the results from the immunohistochemical evaluations, significantly reduced PARK2 with concomitant accumulations of p62 and ubiquitinated proteins were demonstrated in LF from IPF lungs as compared with those in LF from normal lungs ($p < 0.05$, Fig. 7B). We observed no significant increase in the ratio of p-PDGFRs to PDGFRs, which appeared to be due to increased expression levels of PDGFRs. However, a significant increase in the ratio of p-PDGFRs to β-actin indicates that not only expression levels but also PDGFRs activation was enhanced in LF from IPF ($p < 0.05$, Fig. 7B, *right bottom panels*). Although a recent study showed reduced PINK1 expression levels in IPF lung (18), no clear difference of expression levels was demonstrated between normal LF and IPF LF (Fig. 7B). Insufficient mitophagy in IPF LF was

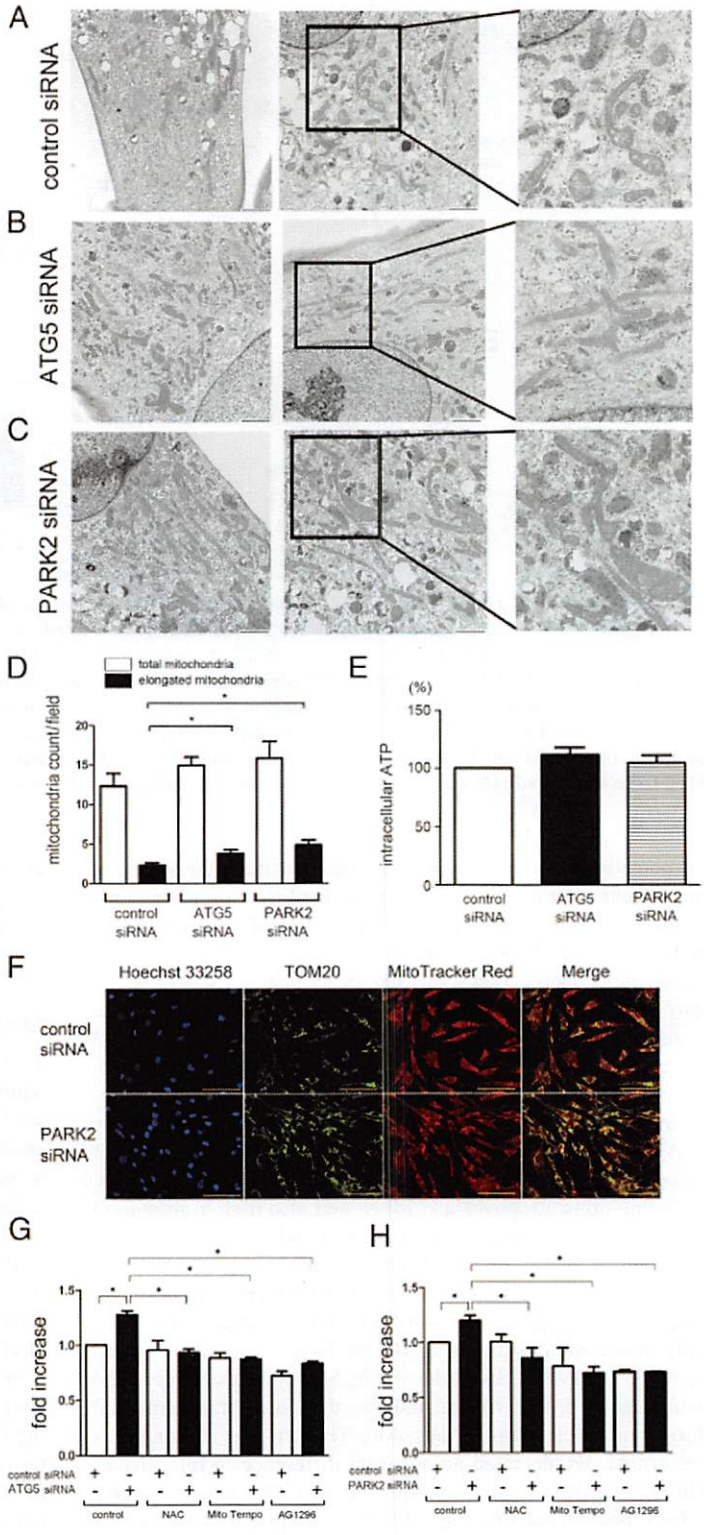

FIGURE 6. Electron microscopic detection of mitochondria, ATP production, and cell proliferation. LF were transfected with control (**A**), ATG5 (**B**), and PARK2 (**C**) siRNA, respectively. (**D**) Shown is the average (±SEM) count of mitochondria taken from a 10-image field (10,000×) for each sample. Open bar is total mitochondria and filled bar is elongated mitochondria. $*p < 0.05$. Mitochondria >2 μm were counted as elongated. (**E**) Intracellular ATP levels were determined after transfection with control (open bar), ATG5 (filled bar), and PARK2 siRNA (horizontal crosshatched bar). The ATP levels in the cells transfected with control siRNA were set at 100%. (**F**) Images of Hoechst 33258, TOM20, and MitoTracker Red staining in LF. The *upper panels* are control siRNA transfected and *lower panels* are PARK2 siRNA transfected. MitoTracker Red staining was started at 48 h posttransfection. Scale bars, 100 μm. (**G**) Cell proliferation was evaluated by MTT assay. LF were transfected with control and ATG5 siRNA, respectively. NAC (1 mM), Mito-TEMPO (100 μM), and AG1296 (15 μM) treatments were started at 24 h posttransfection and cell proliferation was assessed after 48 h of treatment. Open bar is control siRNA and filled bar is ATG5 siRNA. $*p < 0.05$. (**H**) Cell proliferation was evaluated by MTT assay. LF were transfected with control and PARK2 siRNA, respectively. NAC (1 mM), Mito-TEMPO (100 μM), and AG1296 (15 μM) treatments were started at 24 h posttransfection and cell proliferation was assessed after 48 h of treatment. Open bar is control siRNA and filled bar is PARK2 siRNA. $*p < 0.05$.

further demonstrated by the findings of enhanced MitoSOX Red staining (Fig. 7C). Taken together, these findings suggest the physiologically relevant causal link between reduced PARK2-mediated insufficient mitophagy and PDGFRs activation in FF in IPF.

Enhancement of BLM-induced lung fibrosis in the PARK2 knockout mouse

To further clarify the biological relevance of impaired mitophagy-mediated myofibroblast differentiation in lung fibrosis development, we employed BLM-induced lung fibrosis models in the PARK2 knockout (KO) mouse. To show the involvement of PDGFRs signaling during lung fibrosis development, i.p. AG1296 injection was initiated on day 8 after BLM treatment. In general, day 8 is considered to be the beginning of the fibrotic phase with concomitant resolution of acute inflammatory reaction in BLM models. BLM-treated PARK2 KO mice demonstrated augmentation of lung fibrosis development, which was examined by means of Masson trichrome staining (Fig. 8A, 8B) and Sircol collagen assay at day 21 (wild-

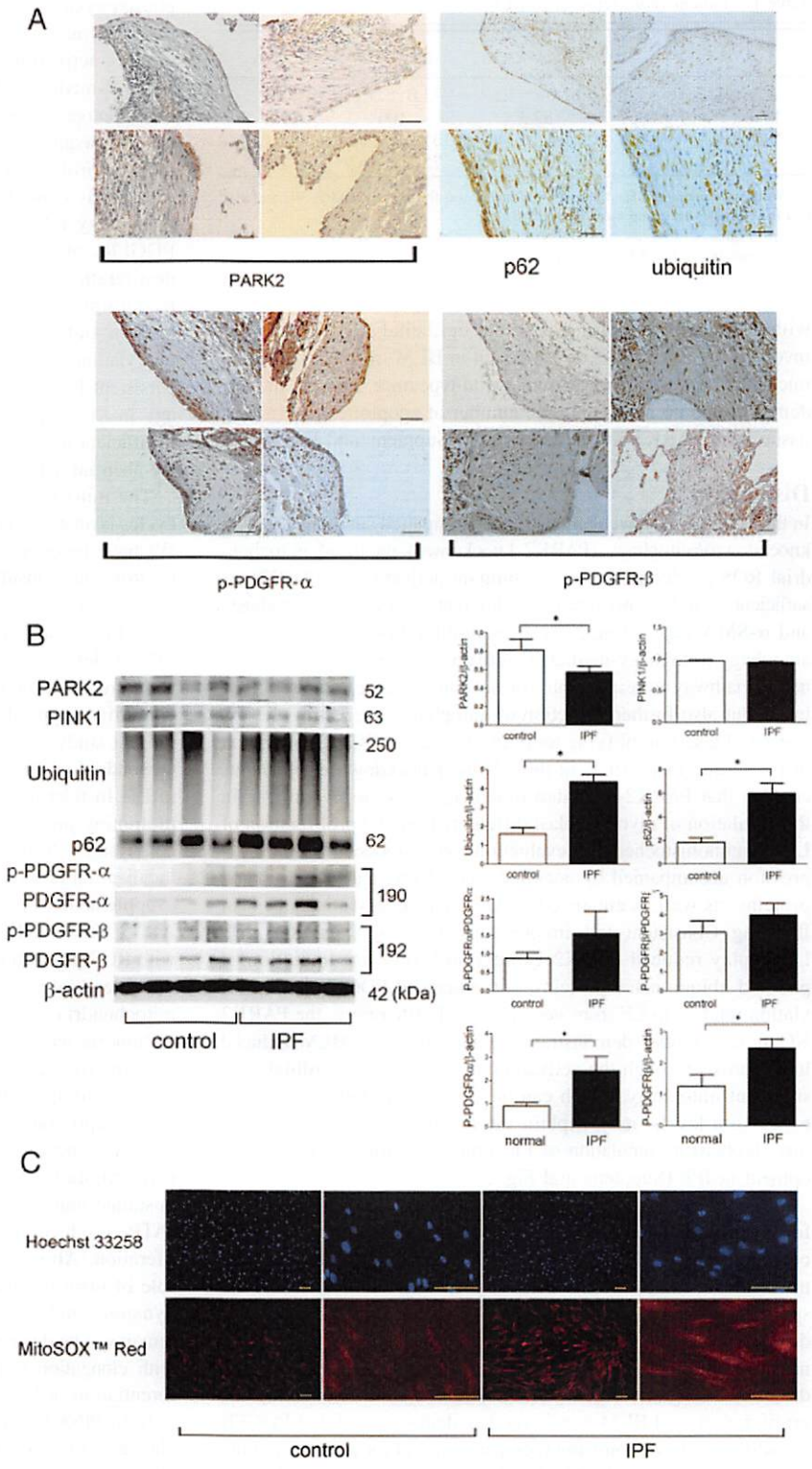

FIGURE 7. PARK2 expression and mitophagy in IPF lung tissues and LF derived from IPF lung. (**A**) Immunohistochemical staining of PARK2 ($n = 4$), p62 ($n = 2$), ubiquitin ($n = 2$), p–PDGFR-α ($n = 4$), and p–PDGFR-β ($n = 4$) in IPF lung tissues: photomicrographs of fibroblastic focus (FF) in IPF. Scale bars, 50 μm. (**B**) Western blot using anti-PARK2, anti-PINK1, anti-ubiquitin, anti-p62, anti–p-PDGFR-α, anti–PDGFR-α, anti–p-PDGFR-β, anti–PDGFR-β, and anti–β-actin of cell lysates from LF isolated from control normal lung (*lanes 1–4*) and from IPF lung (*lanes 5–8*). In the *right panels* are the averages (±SEM) shown as relative expression. Open bar is control LF from normal lung and filled bar is LF from IPF lung. $*p < 0.05$. (**C**) Images of Hoechst 33258 and MitoSOX Red fluorescence staining in LF. Scale bars, 100 μm.

type BLM 1.30 mg/lung on average versus PARK2 KO BLM 1.93 mg/lung on average, $p = 0.0236$, Fig. 8C). Enhanced lung fibrosis in BLM-treated PARK2 KO mice was efficiently attenuated by the injection of AG1296 and was comparable to levels seen in AG1296-injected BLM-treated wild-type mice (Fig. 8A, 8B) (wild-type BLM with AG1296 1.23 mg/lung on average versus PARK2 KO BLM with AG1296 1.24 mg/lung on average, Fig. 8C), suggesting that PDGFR signaling is mainly responsible for enhanced fibrosis development in BLM-treated PARK2 KO mice. Immunohistochemical evaluation elucidated increased expression levels of the phosphorylated form of PDGFRs in PARK2 KO mice, which was apparently suppressed by injection of AG1296 (Fig. 8D). Enhanced PDGFR signaling in the BLM-treated PARK2 KO mouse was further confirmed by means of Western blotting using lung homogenates ($p < 0.05$; Fig. 8E). A recent study showed that PINK1 deficiency–mediated mitophagy impairment is associated

Table I. Patient characteristics (for LF)

	Control (n = 6)	IPF (n = 6)	p Value
Age (y)	67.0 ± 7.2	71.0 ± 5.1	NS
Males (% of group)	83.3	100	NS
SI (pack y)	33.6 ± 14.1	131.2 ± 99.6*	<0.05
% VC	115.8 ± 15.2	75.1 ± 16.9*	<0.05

Values are mean ± SD. A Mann–Whitney U test for age, SI, and % VC and a χ^2 test for % males in group were performed.
*$p < 0.05$.
SI, smoking index; VC, vital capacity.

with enhanced apoptosis in alveolar epithelial cells, which was involved in lung fibrosis development in BLM-treated PINK1 KO mice (18). However, compared with wild-type mice, TUNEL staining demonstrated no increase in the number of apoptotic cells in lung tissue from PARK2 KO mice at day 7 (Supplemental Fig. 2).

Discussion

In the present study, we demonstrate that impaired autophagy (ATG5 knockdown)/mitophagy (PARK2 knockdown)–mediated mitochondrial ROS production with concomitant activation of PDGFRs is sufficient to induce myofibroblast differentiation of type I collagen and α-SMA expression, as well as proliferation in LF. Reduced autophagy/mitophagy-mediated activation of the PDGFRs signaling pathway is responsible for not only phenotypic alterations in LF but also further reduction of autophagy, suggesting the existence of a self-amplifying loop for persistent PDGFRs activation in the setting of insufficient mitophagy. Knockdown experiments confirm that PARK2-mediated mitophagy plays a pivotal role in the regulation of myofibroblast differentiation and proliferation of LF. Immunohistochemical evaluations show reduced PARK2 expression accompanied by accumulation of p62 and ubiquitinated proteins, as well as enhanced PDGFR phosphorylation in FF in IPF lung. Consistent with immunohistochemical evaluations, IPF LF display reduced PARK2 expression levels, accumulation of p62 and ubiquitinated proteins, and enhanced PDGFR phosphorylation relative to LF from normal lung. Furthermore, the PARK2 KO mouse model demonstrates enhancement of BLM-induced lung fibrosis through the activation of PDGFRs. Accordingly, insufficient mitophagy, which can be attributed to reduced PARK2 expression levels, may explain the mechanisms for pathogenic myofibroblast accumulation of FF formation during fibrosis development in IPF (Supplemental Fig. 3).

Although multiple cell types have been proposed as the source for myofibroblast accumulation in IPF pathogenesis, the extent of contribution by each cell type to the formation of FF remains controversial (2, 5). Hence, rather than a specific cell type being responsible for FF, it is likely that specific pathways of myofibroblast differentiation and proliferation are essential pathogenic components for FF formation. PDGF has been widely implicated in fibrotic disorders through the regulation of myofibroblast differentiation and proliferation, and BLM mouse models demonstrated that PDGFR signaling can be a promising therapeutic target for preventing lung fibrosis development (12–15, 29–31). In terms of clinical relevance of PDGFR signaling in IPF pathogenesis, one of the representative target receptors of nintedanib, a multiple tyrosine kinase inhibitor causing significant reduction in the decline of forced vital capacity for IPF patients, is PDGFR (32). In the present study, immunohistochemical evaluations of FF in IPF lungs and Western blotting of isolated LF from IPF patients demonstrated increased phosphorylation of PDGFRs (Fig. 7). Although the source of ROS remains uncertain, protein phosphatase inactivation via thiol oxidation by ROS has been proposed as the mechanism for PDGFR autophosphorylation (22, 33). Intriguingly, a recent study demonstrated that ROS may indirectly phosphorylate PDGFR through Src family kinases activation in the absence of PDGF (11). Furthermore, PDGFR-mediated downstream signaling of mTOR activation inhibits autophagy with concomitant mitochondrial ROS accumulation, subsequently resulting in an ROS-mediated self-perpetuating loop of prolonged activation of monomeric PDGFRα (11). At least partly consistent with those observations, we elucidated that mitophagy inhibition-derived ROS were crucially involved in PDGFRs phosphorylation, leading to α-SMA expression and proliferation (Figs. 1, 3, 6). The PDGFRs signaling pathway was responsible for further inhibition of autophagy, and both wortmannin and AKT1/2 kinase inhibitor attenuated PDGFRs phosphorylation, suggesting the existence of a self-amplifying loop for persistent PDGFRs activation in the setting of insufficient mitophagy in LF (Supplemental Fig. 3). Accordingly, we speculate that insufficient mitophagy is at least partly involved in the mechanisms for aberrant activation of PDGFR signaling in IPF pathogenesis.

The mitochondrial dynamic of continuous fusion and fission cycles is an essential quality control system for mitochondria (34). We have reported that accumulation of fragmented mitochondria is attributed to insufficient mitophagy in human bronchial epithelial cells, especially in the setting of cigarette smoke extract exposure (26). In line with our findings, a recent study demonstrated that PINK1 deficiency–mediated insufficient mitophagy was responsible for accumulation of dysmorphic and dysfunctional mitochondria in type II alveolar epithelial cells (18). However, in the present study, we showed a significant increase in elongated mitochondrial counts in the setting of ATG5 and PARK2 knockdown in LF. In relationship to expression levels of fusion- and fission-promoting proteins, no apparent alteration was observed in total cell lysates during PARK2 knockdown, and thus mitochondrial localization of those proteins should be examined in future studies (Supplemental Fig. 1). We speculate that mitophagy inhibition by ATG5 and PARK2 knockdown induces mitochondrial damage with ROS production, which is sufficiently rescued by an enhanced mitochondrial fusion process, resulting in an increase in elongated mitochondria without apparent accumulation of dysmorphic mitochondria with swelling and crista disruption as shown by electron microscopy evaluation (Fig. 6). Mitochondria elongation resulting from insufficient mitophagy may be associated with metabolic reprogramming of mitochondria, which has been demonstrated to be involved in the mechanisms for TGF-β–induced myofibroblast differentiation (35). Therefore, it is reasonable to postulate that elongated mitochondria are responsible for energy (ATP) production during myofibroblast differentiation and proliferation. Although a cell type–specific and stimulus-dependent role of insufficient mitophagy in the regulation of mitochondrial dynamics and cell fate, including cell death and differentiation, remains to be determined, the lesser extent of mitochondrial damage with elongation is likely to be associated with myofibroblast differentiation in LF.

Both PINK1 and PARK2 are essential for mitophagy and mitochondrial ROS regulation (25). It has been reported that mitophagy inhibition by genetic deletion of *PINK1* can be rescued by transgenic PARK2 expression, but not vice versa, indicating the pivotal role of PARK2 in mitophagy regulation (36). Our in vitro experiments elucidated that PARK2 knockdown more efficiently induced myofibroblast differentiation than that observed by PINK1 knockdown (Fig. 2). A recent study showed that PINK1 deficiency–induced insufficient mitophagy was mainly involved in the regulation of alveolar epithelial cell apoptosis, but no phenotypic alterations in fibroblasts isolated from PINK1 KO mice were demonstrated (18). We observed no significant reduction of PINK1 expression levels in

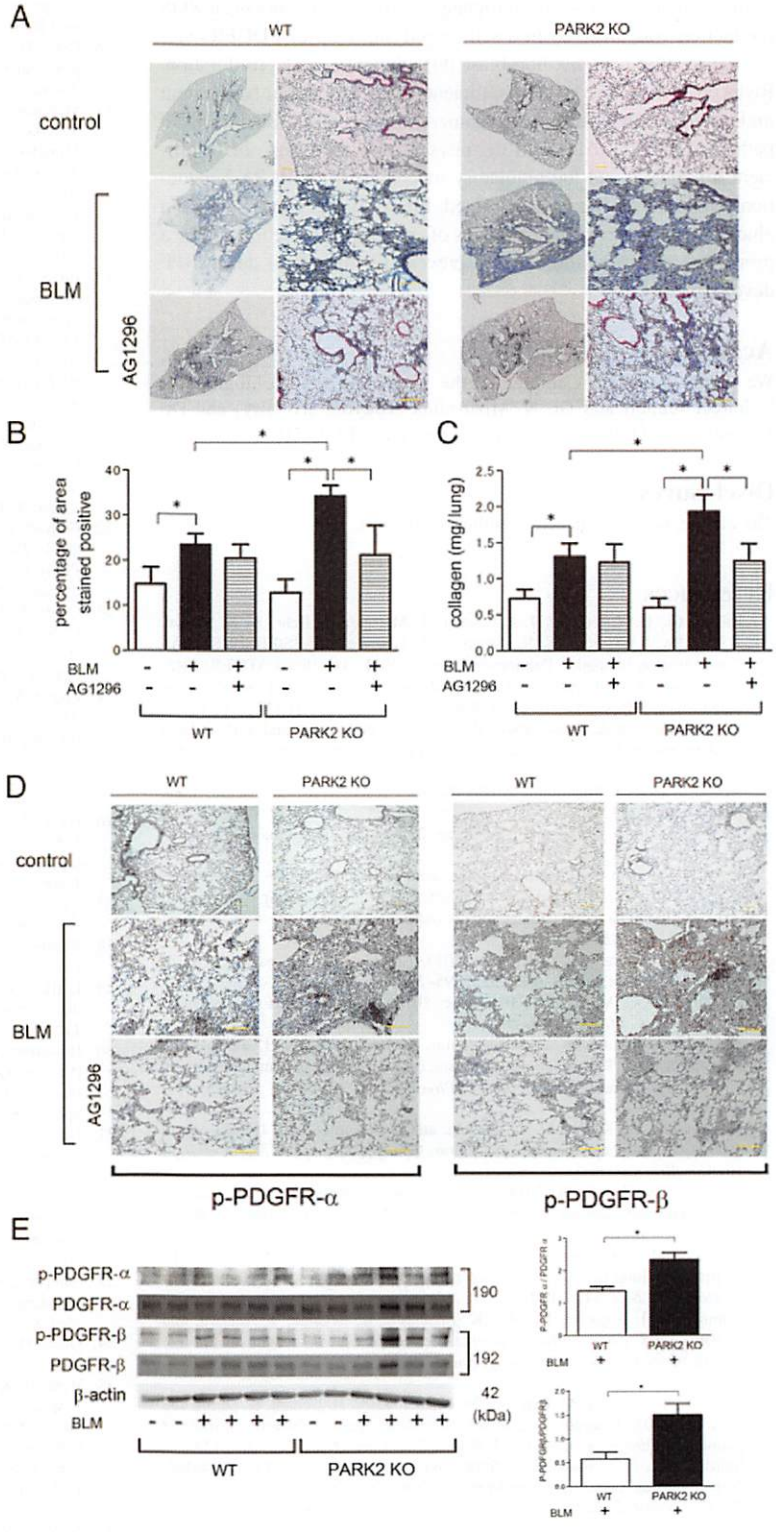

FIGURE 8. BLM-induced lung fibrosis in PARK2 KO mouse. (**A**) Photomicrographs of Masson trichrome staining in control, BLM-treated, and BLM-treated with subsequent AG1296 injection mouse lungs at day 21. Scale bars, 100 μm. (**B**) Shown are the averages (±SEM) of percentage of positively stained area quantified by using ImageJ. Open bar is control, filled bar is BLM treated, and horizontal crosshatched bar is BLM treated with subsequent AG1296 injection. Treatment groups were composed of the same number of mice ($n = 8$). *$p < 0.05$. (**C**) Shown are the average (±SEM) soluble collagen measurements from Sircol assay using control, BLM-treated, and BLM-treated with subsequent AG1296 injection mouse lungs at day 21. Open bar is control, filled bar is BLM treated, and horizontal crosshatched bar is BLM treated with subsequent AG1296 injection. Treatment groups were composed of the same number of mice ($n = 8$). *$p < 0.05$. (**D**) Immunohistochemical staining of p-PDGFR-α, and p-PDGFR-β in control, BLM-treated, and BLM-treated with subsequent AG1296 injection mouse lungs at day 21. Scale bars, 50 μm. (**E**) Western blot using anti–p-PDGFR-α, anti–PDGFR-α, anti–p-PDGFR-β, anti–PDGFR-β, and β-actin of lung homogenates from control and BLM-treated mice. Lung samples were collected at day 21. The panels are the averages (±SEM) shown as relative expression. Open bar is BLM-treated wild-type mice ($n = 6$) and filled bar is BLM-treated PARK2 KO mice ($n = 6$). *$p < 0.05$.

IPF LF (Fig. 7B). Accordingly, compared with PINK1, it is likely that PARK2 has a predominant role in the regulation of myofibroblast differentiation through mitophagy modulation in IPF LF.

We have reported reduced PARK2 expression levels in association with insufficient mitophagy and epithelial cell damages of accelerated cellular senescence as a part of the pathogenesis for chronic obstructive pulmonary disease (19). Accordingly, as reported in the PINK1 KO mice, increase in epithelial cell damage conferred by insufficient mitophagy can be partly responsible for enhanced BLM-induced lung fibrosis in our PARK2 KO mouse model. However, we observed no significant increase in TUNEL$^+$ apoptotic cells (Supplemental Fig. 2) in lung tissue from BLM-treated PARK2 KO mice. Additionally, enhancement of BLM-induced lung fibrosis was efficiently suppressed by treatment with AG1296 from the beginning of the fibrotic phase, further supporting the notion that PDGFR signaling by insufficient mitophagy has an essential regulatory role in lung fibrosis by modulating myofibroblast differentiation and proliferation in PARK2 KO mice.

In summary, insufficient mitophagy-mediated mitochondrial ROS production was involved in a self-amplifying loop of PDGFRs signaling, resulting in myofibroblast differentiation and proliferation. Reduced PARK2-mediated insufficient mitophagy might be a potent underlying mechanism for disorganized fibrosis development in IPF pathogenesis (37). Although the physiological relevance of insufficient mitophagy and the regulatory mechanisms for PARK2 reduction remain to be clearly determined, future studies should focus on elucidating whether sufficient levels of mitophagy induction can be a promising treatment modality to prevent FF formation during IPF development.

Acknowledgments

We thank Stephanie Cambier of the University of Washington for technical support and Dr. N. Mizushima (Tokyo University) and Dr. T. Yoshimori (Osaka University) for providing LC3 cDNA.

Disclosures

The authors have no financial conflicts of interest.

References

1. Raghu, G., H. R. Collard, J. J. Egan, F. J. Martinez, J. Behr, K. K. Brown, T. V. Colby, J. F. Cordier, K. R. Flaherty, J. A. Lasky, et al; ATS/ERS/JRS/ALAT Committee on Idiopathic Pulmonary Fibrosis. 2011. An official ATS/ERS/JRS/ALAT statement: idiopathic pulmonary fibrosis: evidence-based guidelines for diagnosis and management. *Am. J. Respir. Crit. Care Med.* 183: 788–824.
2. Selman, M., and A. Pardo. 2014. Revealing the pathogenic and aging-related mechanisms of the enigmatic idiopathic pulmonary fibrosis. an integral model. *Am. J. Respir. Crit. Care Med.* 189: 1161–1172.
3. Araya, J., and S. L. Nishimura. 2010. Fibrogenic reactions in lung disease. *Annu. Rev. Pathol.* 5: 77–98.
4. King, T. E., Jr., A. Pardo, and M. Selman. 2011. Idiopathic pulmonary fibrosis. *Lancet* 378: 1949–1961.
5. Hung, C., G. Linn, Y. H. Chow, A. Kobayashi, K. Mittelsteadt, W. A. Altemeier, S. A. Gharib, L. M. Schnapp, and J. S. Duffield. 2013. Role of lung pericytes and resident fibroblasts in the pathogenesis of pulmonary fibrosis. *Am. J. Respir. Crit. Care Med.* 188: 820–830.
6. Araya, J., H. Hara, and K. Kuwano. 2013. Autophagy in the pathogenesis of pulmonary disease. *Intern. Med.* 52: 2295–2303.
7. Kroemer, G., G. Mariño, and B. Levine. 2010. Autophagy and the integrated stress response. *Mol. Cell* 40: 280–293.
8. Araya, J., J. Kojima, N. Takasaka, S. Ito, S. Fujii, H. Hara, H. Yanagisawa, K. Kobayashi, C. Tsurushige, M. Kawaishi, et al. 2013. Insufficient autophagy in idiopathic pulmonary fibrosis. *Am. J. Physiol. Lung Cell. Mol. Physiol.* 304: L56–L69.
9. Nakatogawa, H., K. Suzuki, Y. Kamada, and Y. Ohsumi. 2009. Dynamics and diversity in autophagy mechanisms: lessons from yeast. *Nat. Rev. Mol. Cell Biol.* 10: 458–467.
10. Siani, A., and N. Tirelli. 2014. Myofibroblast differentiation: main features, biomedical relevance, and the role of reactive oxygen species. *Antioxid. Redox Signal.* 21: 768–785.
11. Lei, H., and A. Kazlauskas. 2014. A reactive oxygen species-mediated, self-perpetuating loop persistently activates platelet-derived growth factor receptor α. *Mol. Cell. Biol.* 34: 110–122.
12. Homma, S., I. Nagaoka, H. Abe, K. Takahashi, K. Seyama, T. Nukiwa, and S. Kira. 1995. Localization of platelet-derived growth factor and insulin-like growth factor I in the fibrotic lung. *Am. J. Respir. Crit. Care Med.* 152: 2084–2089.
13. Aono, Y., Y. Nishioka, M. Inayama, M. Ugai, J. Kishi, H. Uehara, K. Izumi, and S. Sone. 2005. Imatinib as a novel antifibrotic agent in bleomycin-induced pulmonary fibrosis in mice. *Am. J. Respir. Crit. Care Med.* 171: 1279–1285.
14. Smith, C. L., S. T. Baek, C. Y. Sung, and M. D. Tallquist. 2011. Epicardial-derived cell epithelial-to-mesenchymal transition and fate specification require PDGF receptor signaling. *Circ. Res.* 108: e15–e26.
15. Chen, Y. T., F. C. Chang, C. F. Wu, Y. H. Chou, H. L. Hsu, W. C. Chiang, J. Shen, Y. M. Chen, K. D. Wu, T. J. Tsai, et al. 2011. Platelet-derived growth factor receptor signaling activates pericyte-myofibroblast transition in obstructive and post-ischemic kidney fibrosis. *Kidney Int.* 80: 1170–1181.
16. Corti, O., and A. Brice. 2013. Mitochondrial quality control turns out to be the principal suspect in parkin and PINK1-related autosomal recessive Parkinson's disease. *Curr. Opin. Neurobiol.* 23: 100–108.
17. Mizumura, K., S. M. Cloonan, K. Nakahira, A. R. Bhashyam, M. Cervo, T. Kitada, K. Glass, C. A. Owen, A. Mahmood, G. R. Washko, et al. 2014. Mitophagy-dependent necroptosis contributes to the pathogenesis of COPD. *J. Clin. Invest.* 124: 3987–4003.
18. Bueno, M., Y. C. Lai, Y. Romero, J. Brands, C. M. St Croix, C. Kamga, C. Corey, J. D. Herazo-Maya, J. Sembrat, J. S. Lee, et al. 2015. PINK1 deficiency impairs mitochondrial homeostasis and promotes lung fibrosis. *J. Clin. Invest.* 125: 521–538.
19. Ito, S., J. Araya, Y. Kurita, K. Kobayashi, N. Takasaka, M. Yoshida, H. Hara, S. Minagawa, H. Wakui, S. Fujii, et al. 2015. PARK2-mediated mitophagy is involved in regulation of HBEC senescence in COPD pathogenesis. *Autophagy* 11: 547–559.
20. Araya, J., S. Cambier, J. A. Markovics, P. Wolters, D. Jablons, A. Hill, W. Finkbeiner, K. Jones, V. C. Broaddus, D. Sheppard, et al. 2007. Squamous metaplasia amplifies pathologic epithelial-mesenchymal interactions in COPD patients. *J. Clin. Invest.* 117: 3551–3562.
21. Kabeya, Y., N. Mizushima, T. Ueno, A. Yamamoto, T. Kirisako, T. Noda, E. Kominami, Y. Ohsumi, and T. Yoshimori. 2000. LC3, a mammalian homologue of yeast Apg8p, is localized in autophagosome membranes after processing. *EMBO J.* 19: 5720–5728.
22. Frijhoff, J., M. Dagnell, M. Augsten, E. Beltrami, M. Giorgio, and A. Östman. 2014. The mitochondrial reactive oxygen species regulator p66Shc controls PDGF-induced signaling and migration through protein tyrosine phosphatase oxidation. *Free Radic. Biol. Med.* 68: 268–277.
23. Conte, E., M. Fruciano, E. Fagone, E. Gili, F. Caraci, M. Iemmolo, N. Crimi, and C. Vancheri. 2011. Inhibition of PI3K prevents the proliferation and differentiation of human lung fibroblasts into myofibroblasts: the role of class I p110 isoforms. *PLoS One* 6: e24663.
24. Zhang, Y., and J. H. Yang. 2013. Activation of the PI3K/Akt pathway by oxidative stress mediates high glucose-induced increase of adipogenic differentiation in primary rat osteoblasts. *J. Cell. Biochem.* 114: 2595–2602.
25. Geisler, S., K. M. Holmström, D. Skujat, F. C. Fiesel, O. C. Rothfuss, P. J. Kahle, and W. Springer. 2010. PINK1/Parkin-mediated mitophagy is dependent on VDAC1 and p62/SQSTM1. *Nat. Cell Biol.* 12: 119–131.
26. Hara, H., J. Araya, S. Ito, K. Kobayashi, N. Takasaka, Y. Yoshii, H. Wakui, J. Kojima, K. Shimizu, T. Numata, et al. 2013. Mitochondrial fragmentation in cigarette smoke-induced bronchial epithelial cell senescence. *Am. J. Physiol. Lung Cell. Mol. Physiol.* 305: L737–L746.
27. Passos, J. F., and Tv. Zglinicki. 2012. Mitochondrial dysfunction and cell senescence–skin deep into mammalian aging. *Aging (Albany, NY)* 4: 74–75.
28. Rubinsztein, D. C., G. Mariño, and G. Kroemer. 2011. Autophagy and aging. *Cell* 146: 682–695.
29. LeBleu, V. S., and R. Kalluri. 2011. Blockade of PDGF receptor signaling reduces myofibroblast number and attenuates renal fibrosis. *Kidney Int.* 80: 1119–1121.
30. Hostettler, K. E., J. Zhong, E. Papakonstantinou, G. Karakiulakis, M. Tamm, P. Seidel, Q. Sun, J. Mandal, D. Lardinois, C. Lambers, and M. Roth. 2014. Anti-fibrotic effects of nintedanib in lung fibroblasts derived from patients with idiopathic pulmonary fibrosis. *Respir. Res.* 15: 157.
31. Noskovicova, N., M. Petrek, O. Eickelberg, and K. Heinzelmann. 2015. Platelet-derived growth factor signaling in the lung. From lung development and disease to clinical studies. *Am. J. Respir. Cell Mol. Biol.* 52: 263–284.
32. Richeldi, L., R. M. du Bois, G. Raghu, A. Azuma, K. K. Brown, U. Costabel, V. Cottin, K. R. Flaherty, D. M. Hansell, Y. Inoue, et al; INPULSIS Trial Investigators. 2014. Efficacy and safety of nintedanib in idiopathic pulmonary fibrosis. *N. Engl. J. Med.* 370: 2071–2082.
33. Sampson, N., P. Berger, and C. Zenzmaier. 2012. Therapeutic targeting of redox signaling in myofibroblast differentiation and age-related fibrotic disease. *Oxid. Med. Cell. Longev.* 2012: 458276.
34. Otera, H., and K. Mihara. 2011. Molecular mechanisms and physiologic functions of mitochondrial dynamics. *J. Biochem.* 149: 241–251.
35. Bernard, K., N. J. Logsdon, S. Ravi, N. Xie, B. P. Persons, S. Rangarajan, J. W. Zmijewski, K. Mitra, G. Liu, V. M. Darley-Usmar, and V. J. Thannickal. 2015. Metabolic reprogramming is required for myofibroblast contractility and differentiation. *J. Biol. Chem.* 290: 25427–25438.
36. Park, J., S. B. Lee, S. Lee, Y. Kim, S. Song, S. Kim, E. Bae, J. Kim, M. Shong, J. M. Kim, and J. Chung. 2006. Mitochondrial dysfunction in *Drosophila* PINK1 mutants is complemented by parkin. *Nature* 441: 1157–1161.
37. Noble, P. W., and R. J. Homer. 2004. Idiopathic pulmonary fibrosis: new insights into pathogenesis. *Clin. Chest Med.* 25: 749–758.